Original Article

White matter microstructural alterations are associated with cognitive decline in benzodiazepine use disorders: a multi-shell diffusion magnetic resonance imaging study

Meizhi Yi[1#], Tianyao Wang[2#], Xun Li[3#], Yihong Jiang[4], Yan Wang[1], Luokai Zhang[5], Wen Chen[1], Jun Hu[1], Huiting Wu[1], Yang Zhou[6], Guanghua Luo[1], Jun Liu[7], Hong Zhou[1]^

[1]Department of Radiology, The First Affiliated Hospital, Hengyang Medical School, University of South China, Hengyang, China; [2]Department of Radiology, Renji Hospital, Shanghai Jiaotong University School of Medicine, Shanghai, China; [3]Department of Clinical Psychology, The First Affiliated Hospital, Hengyang Medical School, University of South China, Hengyang, China; [4]Radiology Department, Xiangtan Central Hospital, Xiangtan, China; [5]Radiology Department, The Central Hospital of Shaoyang, Shaoyang, China; [6]Department of Neurology, Nanhua Affiliated Hospital, Hengyang Medical School, University of South China, Hengyang, China; [7]Department of Radiology, The Second Xiangya Hospital of Central South University, Changsha, China

Contributions: (I) Conception and design: M Yi, H Zhou, T Wang; (II) Administrative support: H Zhou, J Liu; (III) Provision of study materials or patients: X Li; (IV) Collection and assembly of data: Y Jiang, Y Wang, L Zhang, W Chen, J Hu, H Wu, Y Zhou; (V) Data analysis and interpretation: M Yi, H Zhou, J Liu, T Wang; (VI) Manuscript writing: All authors; (VII) Final approval of manuscript: All authors.

[#]These authors contributed equally to this work.

Correspondence to: Hong Zhou, MD. Department of Radiology, The First Affiliated Hospital, Hengyang Medical School, University of South China, 69 Chuanshan Road, Shigu District, Hengyang 421002, China. Email: hongzhou@usc.edu.cn; Jun Liu, MD. Department of Radiology, The Second Xiangya Hospital of Central South University, 139 Renmin Middle Road, Changsha 410011, China. Email: junliu123@csu.edu.cn.

Background: Benzodiazepine use disorders (BUDs) have become a public health issue that cannot be ignored. We aimed to demonstrate that patients with BUDs might undergo changes in white matter (WM) integrity, which are related to impaired cognitive function.

Methods: We used diffusion tensor imaging (DTI), diffusion kurtosis imaging (DKI), neurite orientation dispersion and density imaging (NODDI), and mean apparent propagator (MAP) to observe changes in WM structure from 29 patients with sleep disorders with BUD (SDBUD), 33 patients with sleep disorders with non-BUD (SDNBUD), and 25 healthy participants. We also compared the diagnostic performance of the diffusion metrics and models in predicting the status of BUDs and evaluated the relationship between WM changes and cognitive impairment.

Results: BUD was closely associated with WM damage in the corpus callosum (CC) and pontine crossing tract (PCT). There were 14 main diffusion metrics that could be used to predict BUD status (P=0.001–0.023). DTI, DKI, NODDI, and MAP had similar satisfactory performance for predicting BUD status (P=0.001–0.021). Pearson correlation analysis showed a close relationship between the Trail Making Test B (TMT-B) and DTI/NODDI metrics in the splenium of the CC and PCT and between the Montreal Cognitive Assessment (MoCA) and MAP metrics in the splenium of the CC in the SDBUD group (P=0.008–0.040).

Conclusions: Our findings provide evidence for the neurobiological mechanism of benzodiazepine addiction and a novel method for the clinical diagnosis of BUDs.

Keywords: Substance use disorders; benzodiazepine; white matter (WM); diffusion magnetic resonance imaging (dMRI)

^ ORCID: 0000-0002-6460-3420.

Submitted Jul 25, 2024. Accepted for publication Jan 17, 2025. Published online Feb 26, 2025.
doi: 10.21037/qims-24-1516
View this article at: https://dx.doi.org/10.21037/qims-24-1516

Introduction

Chronic sleep disorders can cause symptoms such as fatigue, dizziness, lethargy, and general malaise, which seriously affect the social functions of patients. The first-line medical treatment for sleep disorders is benzodiazepines (1). Although short-term use of benzodiazepines is relatively safe, long-term use can lead to drug dependence (2,3). Addiction, abuse, harmful use, and dependence on benzodiazepines are collectively referred to as benzodiazepine use disorders (BUDs) (4). Approximately half of the patients who use benzodiazepines daily for more than 1 month will become dependent on them (4). The increasing prevalence of BUDs among patients with sleep disorders has become a public health issue that cannot be ignored. Currently, our understanding of the neurobiological mechanisms behind BUDs in these patients is extremely limited. Furthermore, the assessment of these disorders still relies heavily on patients' self-reports and clinicians' judgments, which often involve substantial subjectivity and variability and lack precision in prediction and classification (5). Therefore, there is an urgent need for more objective and accurate noninvasive biomarkers to identify the presence and severity of BUDs in patients with sleep disorders.

To date, there is scant neuroimaging research on BUDs in patients with sleep disorders. The existing neuroimaging studies on other substance use disorders have mainly focused on drugs, alcohol, and nicotine. Many of these studies suggest a relationship between substance abuse and the integrity of white matter (WM) (6-8). A preponderance of evidence indicates that individuals who abuse alcohol or opiates generally exhibit lower coherence in connective WM, most often in the major WM fiber pathways such as the corpus callosum (CC) and the superior and inferior longitudinal fasciculus, which are closely related to executive function and metacognition (9-11). Patients with BUDs have also been confirmed to experience a series of cognitive impairments, which may persist even after drug withdrawal (12,13). Benzodiazepines have similar pharmacological effects to alcohol (both act on the γ-aminobutyric acid subtype A receptor) and are the preferred alternative treatment for patients with alcohol use disorders in the acute phase (14,15). We therefore hypothesize that patients with BUDs may also undergo changes in WM integrity similar to those in patients with alcohol use disorders.

To test this hypothesis, we used multi-shell diffusion imaging, including diffusion tensor imaging (DTI), diffusion kurtosis imaging (DKI), neurite orientation dispersion and density imaging (NODDI), and mean apparent propagator (MAP) to compare the integrity of WM in patients with sleep disorders with BUD (SDBUD), patients with sleep disorders with non-BUD (SDNBUD), and healthy participants. As discussed in some previous studies, the relative advantages of categorical and dimensional criteria for classifying the substance use disorders have been debated for many years. At present, the diagnostic criteria of the Diagnostic and Statistical Manual for Mental Disorders Version 5 (DSM-V) mainly rely on behavioral patterns and lack biological validation. This makes the diagnosis of substance use disorders more subjective than objective biomarkers, which can lead to misdiagnosis or missed diagnosis. Thus, we also compared the diagnostic performance of the main diffusion metrics and the four diffusion models in predicting the status of BUDs. Furthermore, we evaluated the relationship between WM structural changes and cognitive impairment in SDBUD and SDNBUD patients. We present this article in accordance with the STROBE reporting checklist (available at https://qims.amegroups.com/article/view/10.21037/qims-24-1516/rc).

Methods

The study was conducted in accordance with the Declaration of Helsinki (as revised in 2013). The study was registered at the Chinese Clinical Trial Register (No. ChiCTR2200057967) and was approved by the institutional ethics review board of The First Affiliated Hospital of the University of South China (No. 2021KS-FS-17-02). The experimental process was clearly explained to the participants, and they signed an informed consent form. A brief summary of the study procedures is shown in *Figure 1*.

Participants

Sleep disorders group

In this study, patients with sleep disorders were recruited

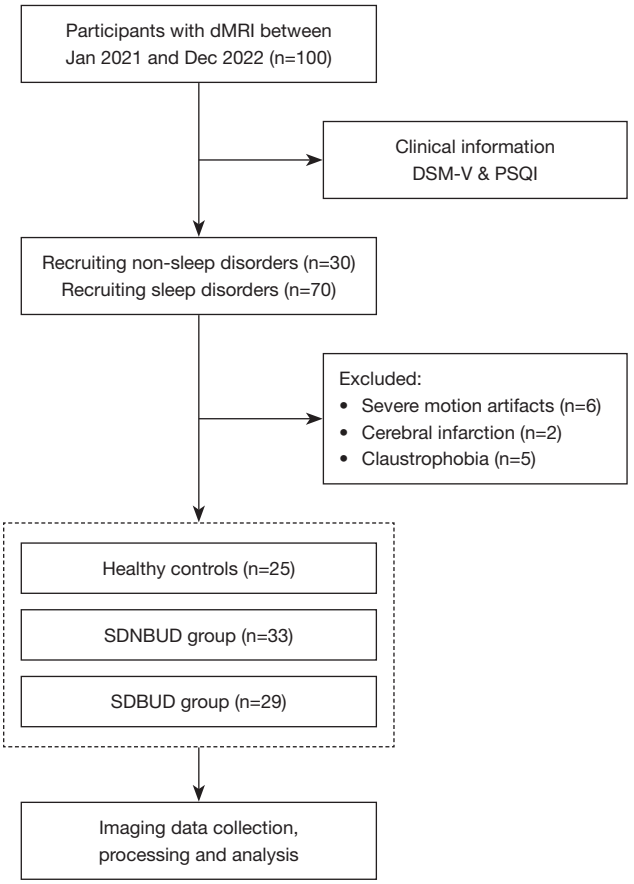

Figure 1 Flowchart of the study procedures. dMRI, diffusion magnetic resonance imaging; DSM-V, Diagnostic and Statistical Manual for Mental Disorders Version 5; PSQI, Pittsburgh Sleep Quality Index; SDNBUD, sleep disorders with non-benzodiazepine use disorder; SDBUD, sleep disorders with benzodiazepine use disorder.

from the outpatient psychological department of The First Affiliated Hospital of the University of South China from January 2021 to December 2022. They were all of Han nationality and right-handed, were between 18 and 70 years old, and had a Pittsburgh Sleep Quality Index (PSQI) score ≥6 points (16). They had normal intelligence and an education level of primary school or above. They did not have neurological disorders, severe chronic disease, serious mental diseases, or contraindications to magnetic resonance imaging (MRI). None of the patients took any other types of psychiatric drugs except benzodiazepines.

According to the diagnostic criteria for sedative drug use disorders in the DSM-V, the sleep disorders group was subdivided into an SDBUD group and an SDNBUD group. After excluding 2 patients with claustrophobia, 29 participants were finally enrolled in the SDBUD group. After excluding 6 patients with severe motion artifacts, 33 participants were included in the SDNBUD group, which contained patients with several simple sleep disorders.

Healthy control (HC) group

The HC group participants were recruited from the community through advertising during the same period as the recruitment of the sleep disorders group. They were all of Han nationality and right-handed, were between 18 and 70 years old, and had PSQI scores <6 points. They had normal intelligence and an education level of primary school or above. The exclusion criteria were the same as those for the sleep disorders group. After excluding 2 patients with a history of cerebral infarction and 3 patients with claustrophobia, 25 participants were included in the HC group.

Clinical scale evaluation

The scales administered and evaluated in this study were completed by two trained residents with 3 years of work experience. The Hamilton Anxiety Scale (HAMA) (17) and Hamilton Depression Scale (HAMD) (18) were used to assess the severity of anxious and depressive states. The Mini-Mental State Examination (MMSE) (19), Montreal Cognitive Assessment (MoCA) (20), and Trail Making Test A and B (TMT-A and TMT-B) (21) were administered to assess changes in the cognitive function of participants.

MRI parameters and image processing

All imaging data were acquired on a Siemens MAGNETOM Prisma 3.0 T scanner (Erlangen, Germany) with a 64-channel head-neck coil at the Radiology Department of The First Affiliated Hospital of the University of South China. All participants underwent T1-weighted (T1W) structural and multi-shell diffusion-weighted imaging (DWI). T1W imaging (T1WI) used a magnetization-prepared rapid gradient-echo (MPRAGE) sequence with the following parameters: resolution =1×1×1 mm^3, repetition time (TR) =2,400 ms, echo time (TE) =2.13 ms, inversion time (TI) =1,000 ms, field of view (FOV) =256×256 mm^2, thickness =1 mm, number of slices =192, flip angle =8°, acquisition time (TA) =5 minutes 45 seconds. DWI scans were acquired using a single-shot echo-planar imaging (EPI) sequence with a multiband, multi-shell acquisition protocol with the following parameters:

resolution =2×2×2 mm^3, TR =2,800 ms, TE =86 ms, FOV =256×256 mm^2, thickness =2 mm, number of slices =76, TA =9 minutes 41 seconds, multiband acceleration factor =4, phase-encoding direction = posterior to anterior. A total of 202 separate volumes were acquired: 10 b=0 s/mm^2 volumes and 192 diffusion-weighted images with three diffusion-weighted shells at b=1,000, 2,000, and 3,000 s/mm^2 (each b-value shell contained 64 diffusion-weighted images). The gradient encoding schemes for multi-shell diffusion MRI (dMRI) data collection were generated using the multi-shelled sampling method reported by Caruyer *et al.* (22). We also acquired another four b=0 s/mm^2 images with the opposite phase-encoding direction (anterior to posterior) to correct for susceptibility distortions. Diffusion-weighted images were preprocessed with the MRtrix3 software package (https://www.mrtrix.org/) as follows: first, denoising and removal of Gibbs ringing were performed. Second, distortion correction, eddy current distortion, and slice-to-volume motion correction were performed by FMRIB's Software Library (FSL) package (https://fsl.fmrib.ox.ac.uk/fsl/docs/). Third, bias field corrections were performed by advanced normalization tools (ANTs).

A total of 16 diffusion metrics from four diffusion models were calculated from multi-shelled diffusion-weighted images. We extracted the b=1,000 s/mm^2 single shell to fit DTI by FSL, used both the b=1,000 and 2,000 s/mm^2 shells to fit DKI by diffusion imaging in Python (DIPY) and used the entire multi-shell dataset to fit NODDI-Bingham by computing the unified device architecture diffusion modeling toolbox (cuDIMOT) and MAP by DIPY. DTI scans were used to calculate fractional anisotropy (FA), mean diffusivity (MD), radial diffusivity (RD), and axial diffusivity (AD) (23). DKI scans were fitted with mean kurtosis (MK), axial kurtosis (AK), and radial kurtosis (RK) by DIPY (24). For NODDI, we calculated the total orientation dispersion index (ODItot), primary direction orientation dispersion index (ODIp), secondary direction orientation dispersion index (ODIs), intracellular volume fraction (Vic), and volume fraction of isotropic water molecules (Viso) (25). For MAP, we evaluated the non-Gaussianity (NG), return-to-origin probability (RTOP), return-to-axis probability (RTAP), and return-to-plane probability (RTPP).

For region of interest (ROI) analysis, first, we extracted all B0 volumes and extracted the brain from preprocessed diffusion-weighted images by MRtrix3. Second, T1W images were bias field corrected by N4 bias field correction, and brain tissue was extracted by a brain extraction tool via ANTs. Third, we registered T1W images to the MNI152 standard brain with nonlinear affine registration and registered B0 brains to T1W images with affine methods by ANTs. Then, we applied the Johns Hopkins University (JHU) WM template atlas to transform MNI152 standard space into individual space and extracted the ROIs to obtain the mean value of DWI metrics in individual space.

Statistical analysis

Continuous variables were expressed as the means ± standard deviations. Count variables were presented as frequencies. The normality of the data distribution was determined by the Shapiro-Wilk test, with variance equality checked by Levene's test. When the Shapiro-Wilk test and Levene's test P values were ≥0.05, the continuous variables between each pair of two groups were compared by parametric test. When the Shapiro-Wilk test or Levene's test P value was <0.05, the continuous variables between each pair of groups were compared by the nonparametric test. All the P values were corrected by Bonferroni. The count variables were compared by Chi-squared tests. Univariate and multivariate logistic analyses were used to determine independent predictors of BUD status from dMRI parameters and dMRI models. The cutoff value, sensitivity, specificity, confidence interval (CI), and area under the curve (AUC) of the dMRI parameters were analyzed and calculated. Correlation analysis was performed between the dMRI parameters and the MMSE, MoCA, TMT-A, and TMT-B scores. The statistical analyses were conducted using SPSS software (version 25.0; IBM Corp., Armonk, NY, USA) and the R software package (version 4.3.0; R Foundation for Statistical Computing, Vienna, Austria). Statistical significance was set as a two-sided P value of less than 0.05.

Receiver operating characteristic (ROC) curves were used to assess the ability of dMRI parameters and dMRI models to predict BUD status. The DeLong test was used to observe the difference in the area under the ROC curve using software (MedCalc, version 20.218; MedCalc, Ostend, Belgium). Statistical significance was set as a two-sided P value of less than 0.05.

To investigate the distribution characteristics of the P values of 16 diffusion parameters between each pair of groups in 50 brain regions, a heatmap was created. In the heatmap, each brain region is represented by a row, and each diffusion parameter statistical difference between the two groups is represented by a column. The color at the intersection between the row and column depicts the P value. Color grading is used to visualize the P value, with a

Table 1 Demographic and neuropsychological data across all participants

Demographic and scale evaluation	Groups			P values
	HC (n=25)	SDNBUD (n=33)	SDBUD (n=29)	
Age (years)	52.00±10.62	54.00±7.95	57.00±7.36[¶]	0.011[†]
Gender (F/M)	8/17	23/10[§]	20/9[¶]	0.006[‡]
Education levels (years)	12.00±5.26	9.00±2.88[§]	9.00±2.23	0.002[†]
Cigarette use (yes/no)	8/17	8/25	5/24	0.450[‡]
Alcohol use (yes/no)	7/18	4/29	2/27	0.081[‡]
Diabetes (yes/no)	9/16	8/25	1/28[¶]	0.009[‡]
Hypertension (yes/no)	1/24	5/28	4/25	0.406[‡]
Hyperlipemia (yes/no)	2/23	4/29	2/27	0.810[‡]
Coronary artery disease (yes/no)	1/24	0/33	1/28	0.524[‡]
HAMA (scores)	8.29±6.88	11.32±5.92	12.17±8.35	0.106[†]
HAMD (scores)	6.67±4.95	11.32±7.28	13.69±9.87[¶]	0.014[†]
PSQI (scores)	5.00±1.68	11.00±2.37[§]	14.00±2.37[¶,I]	<0.001[†]
MMSE (scores)	27.00±2.29	26.00±2.93	27.00±1.93	0.071[†]
MoCA (scores)	25.00±4.86	22.00±5.30	23.00±3.84	0.202[†]
TMT-A (s)	45.17±16.89	50.18±22.64	51.07±24.14	0.270[†]
TMT-B (s)	52.80±28.89	69.36±22.69	70.31±32.79[I]	0.049[†]

Unless indicated, all continuous variables were presented as mean ± standard deviation and all count variables were presented as frequency. [†], P values were obtained by one-way ANOVA test among three groups. [‡], P value was obtained by χ^2 test. When the Shapiro-Wilk test and Levene's test P≥0.05, P values between each two groups were acquired by Bonferroni correction. When the Shapiro-Wilk test or Levene's test P<0.05, P values between each two groups were acquired by Kruskal-Wallis test. [§], statistical difference was detected between HC group and SDNBUD group. [¶], statistical difference was detected between HC group and SDBUD group. [I], statistical difference was detected between SDNBUD group and SDBUD group. HC, healthy control; SDNBUD, sleep disorders with non-benzodiazepine use disorders; SDBUD, sleep disorders with benzodiazepine use disorders; F, female; M, male; HAMA, Hamilton Anxiety Scale; HAMD, Hamilton Depression Scale; PSQI, Pittsburgh Sleep Quality Index; MMSE, Mini-Mental State Examination; MoCA, Montreal Cognitive Assessment; TMT-A, Trail Making Test A; TMT-B, Trail Making Test B; ANOVA, analysis of variance.

lighter color representing a lower P value.

Results

Demographic and clinical characteristics of participants

The demographic and clinical characteristics of the participants are shown in *Table 1*. Overall, 87 participants (36 men, 51 women; mean age, 52.57±9.17 years) were included. The PSQI score was significantly different between any pair of groups. There were statistically significant differences between the HC group and the SDBUD group in age, sex, prevalence of diabetes, and HAMD scores (P=0.013, 0.029, 0.002, and 0.014, respectively). There were statistically significant differences between the HC group and the SDNBUD group in sex and education levels (P=0.009 and 0.036). A statistically significant difference was found for TMT-B scores between the SDBUD group and the SDNBUD group (P=0.049). The participants in the SDBUD group had longer completion times on the TMT-B test than those in the SDNBUD group. There were no statistically significant differences in the use of cigarettes and alcohol; the prevalence of hypertension, hyperlipemia, and coronary artery disease; or the HAMA, MMSE, MoCA, and TMT-A scores among the three groups (P≥0.05).

Comparisons of dMRI parameters

The heatmap (*Figure 2*) indicated that the statistically

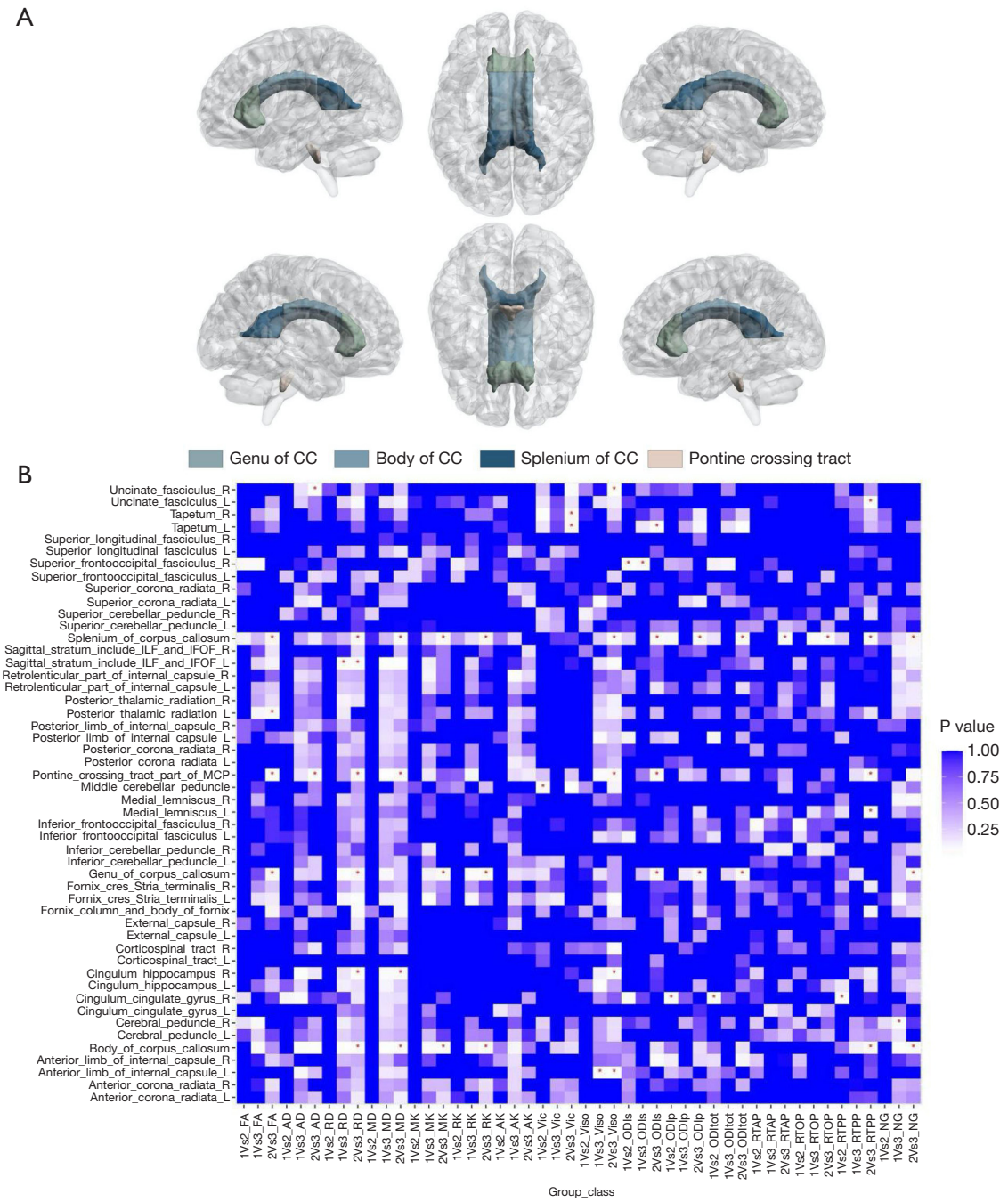

Figure 2 Comparisons of dMRI parameters between each pair of groups. (A) Visualization of the three parts of CC and PCT. (B) Heat map of P values distribution characteristic of 16 diffusion parameters between each two groups in 50 brain regions. *, P value <0.05, Bonferroni corrected. 1 *vs.* 2, HC *vs.* SDNBUDs; 1 *vs.* 3, HC *vs.* SDBUDs; 2 *vs.* 3, SDNBUDs *vs.* SDBUDs. CC, corpus callosum; R, right; L, left; ILF, inferior longitudinal fasciculus; IFOF, inferior fronto-occipital fasciculus; MCP, middle cerebellar peduncle; FA, fractional anisotropy; AD, axial diffusivity; RD, radial diffusivity; MD, mean diffusivity; MK, mean kurtosis; RK, radial kurtosis; AK, axial kurtosis; Vic, intracellular volume fraction; Viso, volume fraction of isotropic water molecules; ODIs, secondary direction orientation dispersion index; ODIp, primary direction orientation dispersion index; ODItot, total orientation dispersion index; RTAP, return-to-axis probability; RTOP, return-to-origin probability; RTPP, return-to-plane probability; NG, non-Gaussianity; dMRI, diffusion magnetic resonance imaging; PCT, pontine crossing tract; HC, healthy control; SDNBUD, sleep disorders with non-benzodiazepine use disorder; SDBUD, sleep disorders with benzodiazepine use disorder.

significant changes in diffusion metrics between each pair of groups were divided into four brain clusters: cluster 1, the genu of the CC; cluster 2, the body of the CC; cluster 3, the splenium of the CC; and cluster 4, the pontine crossing tract (PCT). *Table 2* shows the quantitative comparison of the main dMRI parameters in the four brain areas of the

Table 2 Comparisons of quantitative main diffusion parameters in CC and PCT between groups

Brain clusters	dMRI parameters	Groups			P value[†]
		HC (n=25)	SDNBUD (n=33)	SDBUD (n=29)	
Genu of CC	FA	0.51±0.05	0.51±0.05	0.46±0.08[‡]	0.016
	MD ($\times10^{-3}\cdot mm^2\cdot s^{-1}$)	0.97±0.13	0.95±0.10	1.10±0.22	0.050
	RD ($\times10^{-3}\cdot mm^2\cdot s^{-1}$)	0.68±0.14	0.66±0.12	0.81±0.25[‡]	0.037
	AD ($\times10^{-3}\cdot mm^2\cdot s^{-1}$)	1.54±0.11	1.52±0.09	1.61±0.17	0.137
	MK	0.90±0.06	0.90±0.07	0.85±0.09[‡]	0.019
	RK	1.34±0.13	1.35±0.16	1.24±0.21[‡]	0.022
	AK	0.64±0.04	0.63±0.03	0.62±0.04	0.090
	Vic	0.61±0.03	0.59±0.04	0.60±0.03	0.181
	Viso	0.18±0.06	0.16±0.04	0.22±0.10	0.090
	ODItot	0.16±0.02	0.16±0.02	0.18±0.04[‡]	0.010
	ODIp	0.26±0.02	0.25±0.02	0.28±0.04[‡]	0.011
	ODIs	0.11±0.01	0.10±0.02	0.12±0.03[‡]	0.012
	NG	0.57±0.06	0.56±0.06	0.52±0.07[‡]	0.006
	RTOP ($\times10^{5}\cdot mm^{-3}$)	3.66±4.98	4.69±3.17	4.49±2.58	0.860
	RTPP ($\times10\cdot mm^{-1}$)	5.01±0.29	4.93±0.24	5.25±0.59	0.057
	RTAP ($\times10^{3}\cdot mm^{-2}$)	4.83±11.69	7.35±6.94	7.50±6.90	0.919
Body of CC	FA	0.54±0.04	0.55±0.05	0.50±0.09	0.067
	MD ($\times10^{-3}\cdot mm^2\cdot s^{-1}$)	0.92±0.10	0.91±0.12	1.10±0.32[‡]	0.035
	RD ($\times10^{-3}\cdot mm^2\cdot s^{-1}$)	0.62±0.11	0.60±0.13	0.79±0.35[‡]	0.025
	AD ($\times10^{-3}\cdot mm^2\cdot s^{-1}$)	1.53±0.10	1.53±0.12	1.66±0.25	0.071
	MK	0.94±0.05	0.94±0.07	0.89±0.10[‡]	0.020
	RK	1.52±0.12	1.55±0.18	1.41±0.24[‡]	0.012
	AK	0.64±0.03	0.63±0.03	0.62±0.05	0.182
	Vic	0.62±0.02	0.61±0.03	0.63±0.05	0.181
	Viso	0.16±0.05	0.16±0.05	0.23±0.13	0.073
	ODItot	0.16±0.02	0.15±0.02	0.16±0.03	0.128
	ODIp	0.24±0.02	0.23±0.03	0.25±0.04	0.132
	ODIs	0.11±0.01	0.10±0.02	0.12±0.03	0.143
	NG	0.60±0.05	0.60±0.05	0.56±0.07[‡]	0.010
	RTOP ($\times10^{5}\cdot mm^{-3}$)	4.90±5.36	5.21±3.76	5.65±3.97	0.841
	RTPP ($\times10\cdot mm^{-1}$)	4.95±0.31	4.85±0.27	5.37±0.10[‡]	0.017
	RTAP ($\times10^{3}\cdot mm^{-2}$)	7.24±13.39	8.38±9.32	9.86±9.63	0.580

Table 2 (*continued*)

Table 2 (*continued*)

Brain clusters	dMRI parameters	Groups			P value[†]
		HC (n=25)	SDNBUD (n=33)	SDBUD (n=29)	
Splenium of CC	FA	0.57±0.05	0.60±0.04	0.54±0.08[‡]	0.002
	MD ($\times10^{-3}\cdot mm^2\cdot s^{-1}$)	0.93±0.19	0.88±0.11	1.03±0.29[‡]	0.008
	RD ($\times10^{-3}\cdot mm^2\cdot s^{-1}$)	0.61±0.20	0.55±0.12	0.72±0.31[‡]	0.003
	AD ($\times10^{-3}\cdot mm^2\cdot s^{-1}$)	1.57±0.20	1.56±0.12	1.66±0.25	0.109
	MK	0.90±0.08	0.92±0.08	0.86±0.09[‡]	0.011
	RK	1.40±0.17	1.47±0.18	1.31±0.19[‡]	0.004
	AK	0.60±0.04	0.59±0.03	0.58±0.04	0.124
	Vic	0.64±0.03	0.64±0.04	0.65±0.04	0.664
	Viso	0.17±0.09	0.15±0.05	0.22±0.13[‡]	0.013
	ODItot	0.14±0.20	0.13±0.20	0.14±0.20[‡]	0.008
	ODIp	0.23±0.03	0.22±0.03	0.23±0.03[‡]	0.016
	ODIs	0.08±0.02	0.08±0.02	0.09±0.02[‡]	0.013
	NG	0.63±0.06	0.65±0.05	0.60±0.06[‡]	0.006
	RTOP ($\times10^{5}\cdot mm^{-3}$)	13.00±6.48	12.48±7.95	17.11±6.65[‡]	0.028
	RTPP ($\times10\cdot mm^{-1}$)	4.94±0.68	4.68±0.27	5.12±0.82[‡]	0.003
	RTAP ($\times10^{3}\cdot mm^{-2}$)	25.87±15.58	24.16±19.58	36.59±15.31[‡]	0.013
PCT	FA	0.41±0.02	0.41±0.03	0.39±0.03[‡]	0.004
	MD ($\times10^{-3}\cdot mm^2\cdot s^{-1}$)	0.96±0.08	0.96±0.09	1.03±0.13[‡]	0.009
	RD ($\times10^{-3}\cdot mm^2\cdot s^{-1}$)	0.74±0.09	0.74±0.10	0.83±0.14[‡]	0.007
	AD ($\times10^{-3}\cdot mm^2\cdot s^{-1}$)	1.39±0.08	1.38±0.08	1.44±0.11[‡]	0.025
	MK	0.92±0.04	0.91±0.06	0.89±0.06	0.148
	RK	1.28±0.09	1.24±0.13	1.21±0.11	0.140
	AK	0.71±0.02	0.71±0.02	0.70±0.03	0.067
	Vic	0.60±0.02	0.59±0.03	0.60±0.03	0.216
	Viso	0.17±0.04	0.17±0.04	0.20±0.05[‡]	0.005
	ODItot	0.24±0.02	0.23±0.02	0.23±0.02	0.111
	ODIp	0.35±0.02	0.35±0.02	0.34±0.02	0.203
	ODIs	0.14±0.01	0.14±0.01	0.15±0.01[‡]	0.047
	NG	0.49±0.04	0.48±0.04	0.46±0.03	0.051
	RTOP ($\times10^{5}\cdot mm^{-3}$)	3.36±3.20	3.31±1.67	3.95±1.98	0.698
	RTPP ($\times10\cdot mm^{-1}$)	5.54±0.31	5.41±0.33	5.65±0.45[‡]	0.029
	RTAP ($\times10^{3}\cdot mm^{-2}$)	4.66±7.32	4.79±3.75	6.46±4.50	0.753

All continuous variables were presented as mean ± standard deviation. [†], P values were obtained by comparing among three groups; [‡], statistical difference was detected between the SDNBUD group and SDBUD group. CC, corpus callosum; PCT, pontine crossing tract; dMRI, diffusion magnetic resonance imaging; HC, healthy control; SDNBUD, sleep disorders with non-benzodiazepine use disorders; SDBUD, sleep disorders with benzodiazepine use disorders; FA, fractional anisotropy; MD, mean diffusivity; RD, radial diffusivity; AD, axial diffusivity; MK, mean kurtosis; RK, radial kurtosis; AK, axial kurtosis; Vic, intracellular volume fraction; Viso, volume fraction of isotropic water molecules; ODItot, total orientation dispersion index; ODIp, primary direction orientation dispersion index; ODIs, secondary direction orientation dispersion index; NG, non-Gaussianity; RTOP, return-to-origin probability; RTAP, return-to-axis probability; RTPP, return-to-plane probability.

HC group, SDNBUD group, and SDBUD group. In the genu of the CC, FA, MK, RK, and NG were lower in the SDBUD group than in the SDNBUD group (P=0.028, 0.027, 0.037, and 0.030, respectively), whereas the RD, ODItot, ODIp, and ODIs were higher (P=0.046, 0.008, 0.012, and 0.009, respectively). In the body of the CC, the MK, RK, and NG were lower in the SDBUD group than in the SDNBUD group (P=0.020, 0.013, and 0.018, respectively), whereas the MD, RD, and RTPP were higher (P=0.033, 0.021, and 0.013, respectively). In the splenium of the CC, the FA, MK, RK, and NG were lower in the SDBUD group than in the SDNBUD group (P=0.001, 0.009, 0.002, and 0.005, respectively), whereas the MD, RD, Viso, ODItot, ODIp, ODIs, RTOP, RTPP, and RTAP were higher (P=0.009, 0.002, 0.020, 0.011, 0.039, 0.015, 0.038, 0.004, and 0.016, respectively). In the PCT, the FA values were lower in the SDBUD group than in the SDNBUD group (P=0.023), whereas the MD, RD, AD, Viso, ODIs, and RTPP were higher (P=0.008, 0.007, 0.030, 0.006, 0.042, and 0.024, respectively). No statistically significant differences were found in other dMRI parameters among the three groups in the three parts of the CC and the PCT (P≥0.05).

Diagnostic performance

ROC analyses of the dMRI parameters in different parts of the CC and the PCT in discriminating BUD status are shown in *Table 3*. We analyzed only the dMRI parameters that presented statistically significant differences between the SDBUD and SDNBUD groups. In the genu of the CC, FA, RD, MK, RK, ODItot, ODIp, ODIs, and NG were independent predictors of BUD status (P<0.05). The AUCs of these dMRI parameters ranged from 0.669 to 0.725. Among all the above parameters, ODItot had the highest AUC of 0.725. In the body of the CC, MD, RD, MK, RK, NG, and RTPP were independent predictors of BUD status (P<0.05). The AUCs of these dMRI parameters ranged from 0.673 to 0.704. Among all the above parameters, RTPP had the highest AUC of 0.704. In the splenium of the CC, FA, MD, RD, MK, RK, Viso, ODItot, ODIp, ODIs, NG, RTOP, RTPP, and RTAP were independent predictors of BUD status (P<0.05). The AUCs of these dMRI quantitative parameters ranged from 0.681 to 0.748. Among all the above parameters, FA had the highest AUC of 0.748. In the PCT, FA, MD, RD, AD, Viso, ODIs, and RTPP were independent predictors of BUD status (P<0.05). The AUCs of these dMRI quantitative parameters ranged from 0.323 to 0.730. Among all the above parameters, RD had the highest AUC of 0.730. There were no statistically significant differences in the capacities of the above dMRI parameters for predicting BUD status in the three parts of the CC and the PCT (P≥0.05).

Figure 3A shows that in the genu of the CC, DTI, DKI, NODDI, MAP, and the combined model were independent predictors of BUD status (P<0.05). The AUCs of the dMRI models ranged from 0.671 to 0.746. Among all the models, the combined model had the highest AUC of 0.746. In the body of the CC, DTI, DKI, MAP, and the combined model were independent predictors of BUD status (P<0.05). The AUCs of these dMRI models ranged from 0.692 to 0.724 (*Figure 3B*). Among all these models, the combined model had the highest AUC of 0.724. In the splenium of the CC, DTI, DKI, NODDI, MAP, and the combined model were independent predictors of BUD status (P<0.05). The AUCs of the dMRI models ranged from 0.704 to 0.866 (*Figure 3C*). Among all the models, the combined model had the highest AUC of 0.866. In the PCT, DTI, NODDI, MAP, and the combined model were independent predictors of BUD status (P<0.05). The AUCs of these dMRI models ranged from 0.676 to 0.734 (*Figure 3D*). Among all these models, the combined model had the highest AUC of 0.734. There were no statistically significant differences among these models, either individually or in combination, in the capacity to predict BUD status (P≥0.05).

Partial correlation analysis

In this study, after excluding the effects of age, sex, educational level, drinking and smoking history, underlying diseases, and degrees of anxiety and depression, we conducted a partial correlation analysis of dMRI parameters with cognitive function scales in the SDBUD and SDNBUD groups. We analyzed only the dMRI parameters that presented statistically significant differences between the SDBUD and SDNBUD groups. There was no correlation discovered between the diffusion metrics and cognition scale scores in the SDNBUD group. In the SDBUD group, Pearson correlation analysis in the splenium of the CC (*Figure 4A*) showed that ODItot and ODIp were positively correlated with TMT-B scale scores (r=0.440, P=0.022; r=0.470, P=0.009), and Viso and MD were negatively correlated with TMT-B scale scores (r=–0.470, P=0.008; r=–0.460, P=0.009). RTAP was positively correlated with the MoCA scale scores (r=0.390, P=0.027). In the PCT (*Figure 4B*), AD, MD, RD, and

Table 3 ROC analyses of dMRI parameters of CC and PCT in discriminating BUDs status

Brain clusters	dMRI parameters	Cutoff value	Sensitivity (%)	Specificity (%)	AUC	95% CI	P values
Genu of CC	FA	0.489	58.62	72.73	0.687	0.5531–0.8199	0.012
	RD ($\times10^{-3}\cdot mm^2\cdot s^{-1}$)	0.680	65.52	69.70	0.680	0.5432–0.8174	0.015
	MK	0.788	34.48	100	0.669	0.5315–0.8060	0.023
	RK	1.363	79.31	48.48	0.669	0.5328–0.8047	0.023
	ODItot	0.165	68.97	78.79	0.725	0.5933–0.8571	0.002
	ODIp	0.261	65.52	78.79	0.719	0.5905–0.8473	0.003
	ODIs	0.106	68.97	84.85	0.716	0.5804–0.8511	0.004
	NG	0.564	82.76	54.55	0.671	0.5356–0.8061	0.021
Body of CC	MD ($\times10^{-3}\cdot mm^2\cdot s^{-1}$)	0.900	65.52	69.70	0.687	0.5520–0.8221	0.012
	RD ($\times10^{-3}\cdot mm^2\cdot s^{-1}$)	0.557	79.31	54.55	0.701	0.5697–0.8316	0.007
	MK	0.973	89.66	45.45	0.690	0.5558–0.8235	0.010
	RK	1.619	89.66	45.45	0.692	0.5593–0.8242	0.010
	NG	0.582	68.97	66.67	0.673	0.5366–0.8093	0.020
	RTPP ($\times10\cdot mm^{-1}$)	4.993	55.17	87.88	0.704	0.5702–0.8384	0.006
Splenium of CC	FA	0.593	86.21	63.64	0.748	0.6236–0.8727	0.001
	MD ($\times10^{-3}\cdot mm^2\cdot s^{-1}$)	0.884	68.97	66.67	0.722	0.5957–0.8474	0.003
	RD ($\times10^{-3}\cdot mm^2\cdot s^{-1}$)	0.568	68.97	75.76	0.747	0.6248–0.8684	0.001
	MK	0.918	86.21	60.61	0.713	0.5814–0.8438	0.004
	RK	1.450	86.21	60.61	0.732	0.6039–0.8590	0.002
	Viso	0.135	82.76	51.52	0.698	0.5686–0.8275	0.008
	ODItot	0.124	82.76	63.64	0.713	0.5816–0.8437	0.004
	ODIp	0.217	75.86	63.64	0.690	0.5557–0.8236	0.010
	ODIs	0.078	72.41	69.70	0.701	0.5694–0.8329	0.007
	NG	0.632	79.31	66.67	0.729	0.6031–0.8556	0.002
	RTOP ($\times10^{5}\cdot mm^{-3}$)	14.910	65.52	66.67	0.681	0.5478–0.8148	0.014
	RTPP ($\times10\cdot mm^{-1}$)	4.669	68.97	69.70	0.738	0.6144–0.8611	0.001
	RTAP ($\times10^{3}\cdot mm^{-2}$)	33.288	58.62	75.76	0.694	0.5624–0.8253	0.009
PCT	FA	0.459	34.00	96.90	0.323	0.1884-0.4591	0.018
	MD ($\times10^{-3}\cdot mm^2\cdot s^{-1}$)	0.951	79.30	75.00	0.729	0.5941-0.8642	0.002
	RD ($\times10^{-3}\cdot mm^2\cdot s^{-1}$)	0.738	79.30	71.90	0.730	0.5973-0.8631	0.002
	AD ($\times10^{-3}\cdot mm^2\cdot s^{-1}$)	1.383	65.50	71.90	0.697	0.5621-0.8312	0.008
	Viso	0.168	79.30	68.70	0.717	0.5833-0.8541	0.004
	ODIs	0.140	89.70	46.90	0.682	0.5435-0.3665	0.015
	RTPP ($\times10\cdot mm^{-1}$)	5.335	75.90	68.70	0.676	0.5456-0.8238	0.014

ROC, receiver operating characteristic; dMRI, diffusion magnetic resonance imaging; CC, corpus callosum; PCT, pontine crossing tract; BUD, benzodiazepine use disorder; AUC, area under the curve; CI, confidence interval; FA, fractional anisotropy; RD, radial diffusivity; MK, mean kurtosis; RK, radial kurtosis; ODItot, total orientation dispersion index; ODIp, primary direction orientation dispersion index; ODIs, secondary direction orientation dispersion index; NG, non-Gaussianity; MD, mean diffusivity; RTPP, return-to-plane probability; Viso, volume fraction of isotropic water molecules; RTOP, return-to-origin probability; RTAP, return-to-axis probability; AD, axial diffusivity.

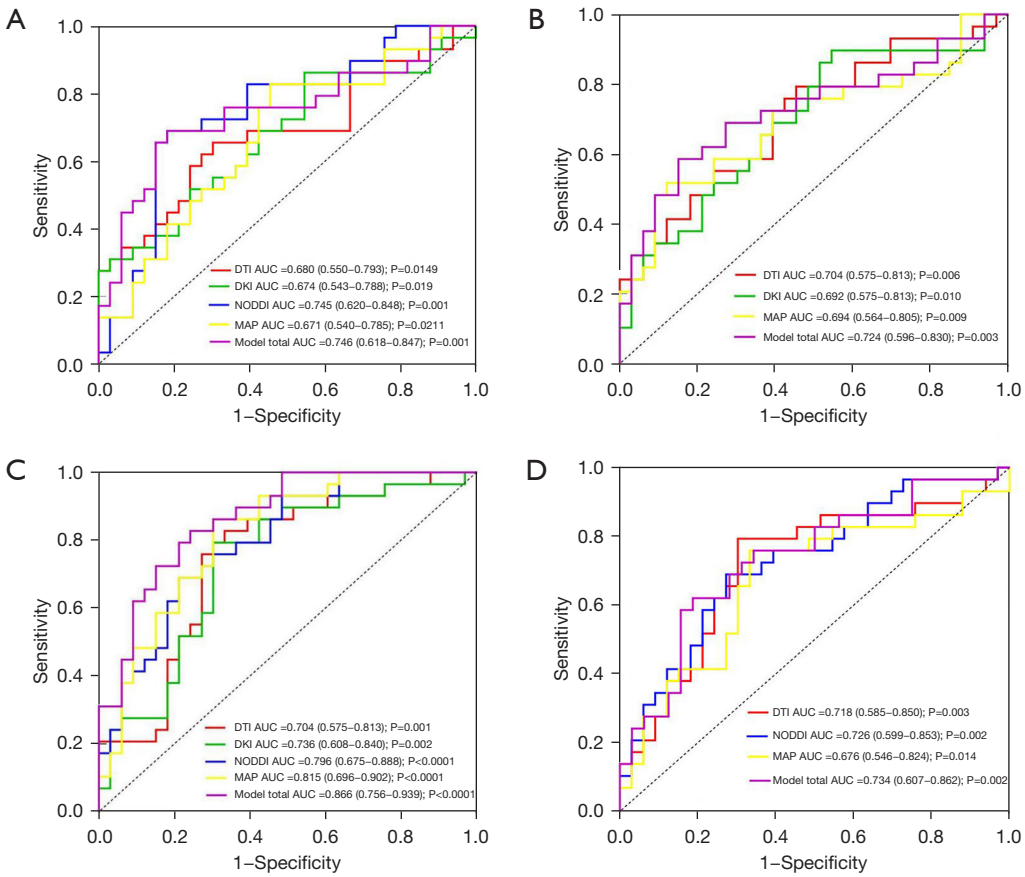

Figure 3 Diagnostic performance of dMRI models to predict BUD status. (A) ROC curves of diffusion models for predicting BUDs status in the genu of CC. (B) ROC curves of diffusion models for predicting BUDs status in the body of CC. (C) ROC curves of diffusion models for predicting BUDs status in the splenium of CC. (D) ROC curves of diffusion models for predicting BUDs status in the PCT. ROC curves were drawn by Prisma. Data in brackets are presented as 95% CI. DTI, diffusion tensor imaging; AUC, area under the curve; DKI, diffusion kurtosis imaging; NODDI, neurite orientation dispersion and density imaging; MAP, mean apparent propagator; dMRI, diffusion magnetic resonance imaging; BUD, benzodiazepine use disorder; CC, corpus callosum; ROC, receiver operating characteristic; PCT, pontine crossing tract; CI, confidence interval.

Viso were negatively correlated with TMT-B scale scores (r=–0.440, P=0.011; r=–0.420, P=0.015; r=–0.410, P=0.021; r=–0.490, P=0.040). *Figure 4C,4D* shows that there were no significant correlations between diffusion metrics and cognitive function scale scores in the genu and body of the CC, respectively (P≥0.05).

Discussion

In this study, the changes in dMRI parameters were a superior reflection of WM abnormalities in three parts of the CC and the PCT, which were related to changes in the cognitive function of the participants in the SDBUD group. Our results strongly supported our initial hypothesis. These findings provide evidence for the neurobiological mechanisms of BUDs. Moreover, our correlation analysis revealed potential clinical implications of these findings for SDBUD patients.

The human CC contains more than 200 million commissural fibers connecting the two hemispheres and is by far the largest WM fiber bundle in the brain (26). It plays a key role in the interhemispheric transmission of sensory, motor, and cognitive functions (27-29). Among these, the cognitive dysfunction caused by microstructural changes in the CC among individuals with alcohol addiction has received increasing attention in recent years (30,31). Several previous

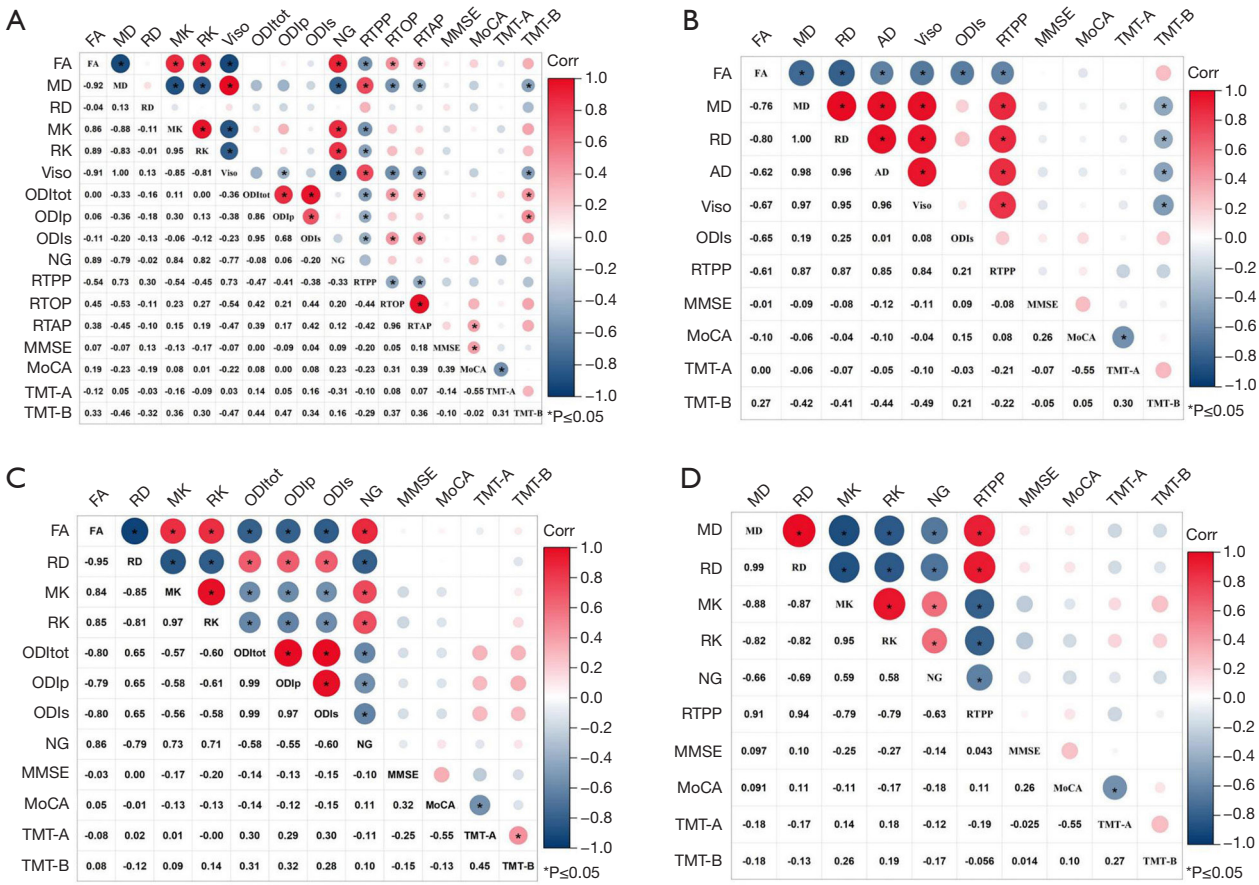

Figure 4 Correlation coefficient between dMRI parameters and cognitive function scales. (A) Heat-map displaying the correlation coefficient between multi-shell diffusion parameters and cognitive function scales in the splenium of CC in SDBUDs. (B) Heat-map displaying the correlation coefficient between multi-shell diffusion parameters and cognitive function scales in the PCT in SDBUDs. (C) Heat-map displaying the correlation coefficient between multi-shell diffusion parameters and cognitive function scales in the genu of CC in SDBUDs. (D) Heat-map displaying the correlation coefficient between multi-shell diffusion parameters and cognitive function scales in the body of CC in SDBUDs. *, there is statistical correlation (P value ≤0.05). Different sizes of the blue and red dots: the larger the dot size, the greater the absolute value of the correlation coefficient. FA, fractional anisotropy; MD, mean diffusivity; RD, radial diffusivity; MK, mean kurtosis; RK, radial kurtosis; Viso, volume fraction of isotropic water molecules; ODItot, total orientation dispersion index; ODIp, primary direction orientation dispersion index; ODIs, secondary direction orientation dispersion index; NG, non-Gaussianity; RTPP, return-to-plane probability; RTOP, return-to-origin probability; RTAP, return-to-axis probability; MMSE, Mini-Mental State Examination; MoCA, Montreal Cognitive Assessment; TMT-A, Trail Making Test A; TMT-B, Trail Making Test B; Corr, correlation coefficient; AD, axial diffusivity; dMRI, diffusion magnetic resonance imaging; CC, corpus callosum; SDBUD, sleep disorders with benzodiazepine use disorder; PCT, pontine crossing tract.

dMRI studies have confirmed these microstructural changes in the CC, not only in patients with alcohol dependence, but also in those with other types of substance misuse (32-35). The PCT is a key component of the ascending reticular activating system from the pontine reticular formation to the thalamus. It is closely related to advanced brain functions such as attention, alertness, introspection, learning, and memory (36). Abnormalities in the WM of this tract are statistically associated with cognitive deficits detectable on neurocognitive testing (37,38).

Compared to the SDNBUD group, there was a reduction in FA of the CC (genu and splenium) and PCT, an increase in MD of the CC (body and splenium) and PCT, an increase in RD of the CC (genu, body, and splenium) and PCT,

and an increase in AD of the PCT in the SDBUD group. These CC findings were consistent with results reported in previous studies on alcohol dependence (32,39,40). Monnig *et al.* found a significant association between the severity of alcoholism ratings and WM FA (41). As alcohol use disorder ratings increased, FA values, as a measure of WM integrity, decreased. This relationship persisted even when controlling for the number of years of drinking. Reduced WM volume was also reported in the pons in normal aging and neuropsychiatric disorders (42). Chronic alcohol consumption can lead to specific neurological disorders involving WM, such as Marchiafava-Bignami disease and central pontine myelinolysis (43). Changes in MD reflect developmental or pathological alterations in the brain tissue caused by changes in the diffusion characteristics of the intracellular and extracellular water compartments, including restricted diffusion and water exchange across permeable boundaries. Reduced FA and increased MD are often detected in most WM regions of individuals exposed to alcohol prenatally, suggesting decreased WM integrity and increased axonal degradation (44,45). Similarly, DTI changes in the three parts of the CC and PCT possibly resulted from damage to WM fibers, which may be caused by edema, demyelination, and axonal loss, a pattern similar to the imaging of children with prenatal alcohol exposure (46,47).

DKI is an advanced, non-Gaussian diffusion imaging measurement that provides a highly accurate diffusion model for quantifying the deviation from the Gaussian distribution, known as kurtosis, in different directions. MK, AK, and RK are the three main kurtosis metrics. A higher kurtosis value indicates that more obstacles are encountered during diffusion and that the area of interest has a higher cell density or cell structure complexity, whereas a reduced peak may mean a loss of cellular structure. Local cerebral ischemic and hypoxic injury, cell membrane damage by massive oxygen radical and lipid peroxidation, and immunoreaction of the organization collaboratively lead to demyelination, reduce the limitation of the medullary sheath on water molecules, and thus decrease the MK value under acute alcohol exposure (48). Our study showed lower MK and RK values in the genu, body, and splenium of the CC in the SDBUD group than in the SDNBUD group. The reduction in diffusion kurtosis values in the SDBUD group may be a result of less synaptic refinement or decreased cell packing, which shares similar neural alterations to those in animal models of alcohol exposure (49,50).

NODDI is based on a "three-compartment tissue model", which allows the distinction of the three types of microstructure environments: intracellular, extracellular, and cerebrospinal fluid chambers. Due to the different molecular diffusion in different chambers, the microstructural changes can be obtained through MRI quantitative metrics. Our results found higher ODItot, ODIp, and ODIs in the CC (genu and splenium) and increased ODIs in the PCT in the SDBUD group compared to the SDNBUD group. Viso in the splenium of the CC and the PCT increased in the SDBUD group compared to the SDNBUD group. In binge drinkers, neurite density was higher in cortical WM in adjacent regions of lower ODI (51). A recent study suggested that although there was a weak relationship between ODI and neurite density, they exhibited a joint disturbance in binge drinkers (52). Increases in ODI in WM regions are indicative of axonal disorganization, degeneration, and dispersion (51,53). Increased Viso is likely indicative of neurodegeneration, wherein the ratio of intracellular to extracellular space is reduced, leading to an increase in the measured fractional volume of extracellular fluid (54).

MAP is a novel diffusion model based on q-space sampling and Hermite function computation that provides several novel, measurable parameters for capturing previously concealed inherent properties of nervous tissue microstructure (55). In our study, a lower NG was found in the genu, body, and splenium of the CC in the SDBUD group than in the SDNBUD group. Similar to MK, decreased NG suggested reduced tissue complexity and was likely a sensitive marker of axonal loss and demyelination, which is related to WM degeneration in AD patients (56). In addition, the RTOP, RTAP, and RTPP in the splenium of the CC in this study showed a slight increase in the SDBUD group relative to the SDNBUD group. The RTPP in the body of CC and the PCT were also observed to be slightly increased in the SDBUD group relative to the SDNBUD group. The zero-displacement probability measures (RTOP, RTAP, and RTPP) are more specific biomarkers for cellularity, the size of cell bodies and processes, or the presence of restricting barriers than MD or the tensor eigenvalues derived with DTI (57). The RTOP parameter can be decomposed in the local anatomical reference system according to the direction of the diffusion tensor into axial and radial. Increased RTPP and RTAP reflect the added presence of restrictive barriers in the axial orientation and radial orientation, respectively (58).

The CC and PCT are characterized not only by demyelination and axonal

disorganization and more axonal restricting barriers in the SDBUD group compared with the SDNBUD group. The above pathological changes possibly coexist rather than occur in isolation, which may explain the contradictory and complicated diffusion features. As few studies have assessed WM integrity in BUDs, especially using a multi-shell diffusion approach, our findings are difficult to compare with prior work. The significant differences in dMRI parameters in these three parts of the CC and the PCT were only present between the SDBUD group and the SDNBUD group. There were no significant differences in dMRI parameters between the SDBUD/SDNBUD group and the HC group. This finding is suggestive of the fact that the magnitude of WM damage in the CC and PCT in SDBUD patients is perhaps at a very early stage and is too slight to be captured. Further research is needed to validate and interpret this supposition.

We also investigated the capacities of the dMRI parameters and the four diffusion models to predict BUD status. Except for Vic and AK, the other 14 diffusion metrics in our study could be individually used to predict BUD status. The predictive capacities of those dMRI parameters showed no statistically significant differences. Similar to the diffusion parameters, all the models could also be used to detect BUD status individually and in combination. Our results showed that the predictive capacities of the four models, individually and in combination, showed no statistically significant differences. The diagnostic performances of the diffusion parameters and diffusion models in this study were similar to the results of previous studies carried out by Gao *et al.* and Crombe *et al.* (59,60). The interpretation of the use of the diffusion metrics and models to confirm BUD status is complicated because different diffusion metrics and models can represent different pathologies and describe different possible attributes. According to the results of our research, DKI, NODDI, and MAP can provide directional and functional complementary information to DTI. However, some prior studies have shown that DKI, NODDI, and MAP are more sensitive than DTI for detecting WM microstructural changes to better understand the process of brain development and aging and for detecting pathological modifications in neurological disorders (61-63). However, these advantages were identified based on technical principles and indirect results, without the direct pathological basis of point-by-point results, indicating the necessity for further research.

The TMT-B scores were slightly elevated in the SDBUD group compared to the SDNBUD group. To some extent, this suggests a minor decline in cognitive function (especially "processing speed" and "cognitive agility") in patients in the SDBUD group. The Pearson correlation analysis showed a close relationship between TMT-B scores and changes in DTI/NODDI metrics in the splenium of the CC and the PCT in the SDBUD group. Additionally, the RTAP of the splenium of the CC had a positive correlation with MoCA scores in the SDBUD group. However, similar correlations were not found in the SDNBUD group. We speculate that the degree of WM structural changes in the splenium of the CC and the PCT may illustrate the severity of cognitive function regression in the SDBUD group.

There are several limitations to this study. Firstly, the relatively small sample size, which cannot be analyzed in different layers, may have introduce bias in comparisons. Secondly, there was a significant variation in the distribution of age and gender between groups, which may have introduced a certain degree of confounding bias. Thirdly, it may be beneficial to analyze additional dMRI metrics to gain a more detailed understanding of brain microstructure, rather than focusing solely on the main metrics in each diffusion model. Finally, it would be of great interest to examine changes in other regional brain areas, including individual functional regions. Therefore, future studies should aim to optimize the entire experimental process.

Conclusions

We report evidence of subtle WM abnormalities in the genu, body, and splenium of the CC and the PCT. Multi-shell diffusion imaging techniques, such as DTI, DKI, NODDI, and MAP, show promise. They have similar satisfactory performance, both individually and in combination, in predicting the status of BUDs. Thus, our findings may provide a novel perspective for the clinical diagnosis and differentiation of BUDs. Changes in DTI, NODDI, and MAP metrics in the splenium of the CC and DTI and NODDI metrics in the PCT are associated with cognitive function damage in SDBUD patients. This may assist in guiding potential clinical treatment strategies in the future.

Acknowledgments

The authors are grateful to all the people who participated in the study. We are thankful for the pleasant cooperation of the six hospitals (The First Affiliated Hospital of

University of South China; The Renji Hospital Affiliated to Shanghai Jiaotong University School of Medicine; The Second Xiangya Hospital of Central South University; The Xiangtan Central Hospital; The Central Hospital of Shaoyang; The Nanhua Affiliated Hospital of University of South China). This manuscript was edited by one or more of the highly qualified native English-speaking editors at American Journal Experts (AJE).

Footnote

Reporting Checklist: The authors have completed the STROBE reporting checklist. Available at https://qims.amegroups.com/article/view/10.21037/qims-24-1516/rc

Funding: This work was supported by the Health Commission Foundation of Hunan Province (Nos. 202209014295 and 202218014518), the Clinical Research 4310 Program of The First Affiliated Hospital of University of South China (No. 20224310NHYCG03), the National Natural Science Foundation of China (No. U22A20303), the Innovative Province special construction foundation of Hunan Province (No. 2020SK4001), the National Natural Science Foundation of China (No. 61971451), and the Science and Technology Innovation Program of Hunan Province (No. 2021RC4016).

Conflicts of Interest: All authors have completed the ICMJE uniform disclosure form (available at https://qims.amegroups.com/article/view/10.21037/qims-24-1516/coif). The authors have no conflicts of interest to declare.

Ethical Statement: The authors are accountable for all aspects of the work in ensuring that questions related to the accuracy or integrity of any part of the work are appropriately investigated and resolved. The study was conducted in accordance with the Declaration of Helsinki (as revised in 2013). The study was approved by the institutional ethics review board of The First Affiliated Hospital of the University of South China (No. 2021KS-FS-17-02). The experimental process was clearly explained to the participants, and they signed an informed consent form.

References

1. Pavlova MK, Latreille V. Sleep Disorders. Am J Med 2019;132:292-9.
2. Lader M. Benzodiazepines revisited--will we ever learn? Addiction 2011;106:2086-109.
3. Lape EC, Powers JM, Hooker JE, Edwards RR, Ditre JW. Benzodiazepine Use and Dependence in Relation to Chronic Pain Intensity and Pain Catastrophizing. J Pain 2023;24:345-55.
4. Soyka M. Treatment of Benzodiazepine Dependence. N Engl J Med 2017;376:1147-57.
5. Padyab M, Armelius BÅ, Armelius K, Nyström S, Blom B, Grönlund AS, Lundgren L. Is Clinical Assessment of Addiction Severity of Individuals with Substance Use Disorder, Using the Addiction Severity Index, A Predictor of Future Inpatient Mental Health Hospitalization? A Nine-Year Registry Study. J Dual Diagn 2018;14:187-91.
6. Hampton WH, Hanik IM, Olson IR. Substance abuse and white matter: Findings, limitations, and future of diffusion tensor imaging research. Drug Alcohol Depend 2019;197:288-98.
7. Albertson DN, Pruetz B, Schmidt CJ, Kuhn DM, Kapatos G, Bannon MJ. Gene expression profile of the nucleus accumbens of human cocaine abusers: evidence for dysregulation of myelin. J Neurochem 2004;88:1211-9.
8. Arnone D, Barrick TR, Chengappa S, Mackay CE, Clark CA, Abou-Saleh MT. Corpus callosum damage in heavy marijuana use: preliminary evidence from diffusion tensor tractography and tract-based spatial statistics. Neuroimage 2008;41:1067-74.
9. Westerhausen R, Kreuder F, Dos Santos Sequeira S, Walter C, Woerner W, Wittling RA, Schweiger E, Wittling W. Effects of handedness and gender on macro- and microstructure of the corpus callosum and its subregions: a combined high-resolution and diffusion-tensor MRI study. Brain Res Cogn Brain Res 2004;21:418-26.
10. Topiwala A, Allan CL, Valkanova V, Zsoldos E, Filippini N, Sexton C, Mahmood A, Fooks P, Singh-Manoux A, Mackay CE, Kivimäki M, Ebmeier KP. Moderate alcohol consumption as risk factor for adverse brain outcomes and cognitive decline: longitudinal cohort study. BMJ

2017;357:j2353.
11. Morie KP, Yip SW, Zhai ZW, Xu J, Hamilton KR, Sinha R, Mayes LC, Potenza MN. White-matter crossing-fiber microstructure in adolescents prenatally exposed to cocaine. Drug Alcohol Depend 2017;174:23-9.
12. Crowe SF, Stranks EK. The Residual Medium and Long-term Cognitive Effects of Benzodiazepine Use: An Updated Meta-analysis. Arch Clin Neuropsychol 2018;33:901-11.
13. Zetsen SPG, Schellekens AFA, Paling EP, Kan CC, Kessels RPC. Cognitive Functioning in Long-Term Benzodiazepine Users. Eur Addict Res 2022;28:377-81.
14. Koob GF. A role for GABA mechanisms in the motivational effects of alcohol. Biochem Pharmacol 2004;68:1515-25.
15. Schuckit MA. Recognition and management of withdrawal delirium (delirium tremens). N Engl J Med 2014;371:2109-13.
16. Buysse DJ, Reynolds CF 3rd, Monk TH, Berman SR, Kupfer DJ. The Pittsburgh Sleep Quality Index: a new instrument for psychiatric practice and research. Psychiatry Res 1989;28:193-213.
17. Hamilton M. The assessment of anxiety states by rating. Br J Med Psychol 1959;32:50-5.
18. Miller IW, Bishop S, Norman WH, Maddever H. The Modified Hamilton Rating Scale for Depression: reliability and validity. Psychiatry Res 1985;14:131-42.
19. Folstein MF, Folstein SE, McHugh PR. "Mini-mental state". A practical method for grading the cognitive state of patients for the clinician. J Psychiatr Res 1975;12:189-98.
20. Nasreddine ZS, Phillips NA, Bédirian V, Charbonneau S, Whitehead V, Collin I, Cummings JL, Chertkow H. The Montreal Cognitive Assessment, MoCA: a brief screening tool for mild cognitive impairment. J Am Geriatr Soc 2005;53:695-9.
21. Reitan RM. Validity of the Trail Making Test as an indicator of organic brain damage. Percept Mot Skills 1958;8:271-6.
22. Caruyer E, Lenglet C, Sapiro G, Deriche R. Design of multishell sampling schemes with uniform coverage in diffusion MRI. Magn Reson Med 2013;69:1534-40.
23. Mukherjee P, Berman JI, Chung SW, Hess CP, Henry RG. Diffusion tensor MR imaging and fiber tractography: theoretic underpinnings. AJNR Am J Neuroradiol 2008;29:632-41.
24. Jensen JH, Helpern JA, Ramani A, Lu H, Kaczynski K. Diffusional kurtosis imaging: the quantification of non-gaussian water diffusion by means of magnetic resonance imaging. Magn Reson Med 2005;53:1432-40.
25. Hernandez-Fernandez M, Reguly I, Jbabdi S, Giles M, Smith S, Sotiropoulos SN. Using GPUs to accelerate computational diffusion MRI: From microstructure estimation to tractography and connectomes. Neuroimage 2019;188:598-615.
26. Tomasch J. Size, distribution, and number of fibres in the human corpus callosum. Anat Rec 1954;119:119-35.
27. Gazzaniga MS. Cerebral specialization and interhemispheric communication: does the corpus callosum enable the human condition? Brain 2000;123:1293-326.
28. Byrne H, Spencer APC, Geary G, Jary S, Thoresen M, Cowan FM, Brooks JCW, Chakkarapani E. Development of the corpus callosum and cognition after neonatal encephalopathy. Ann Clin Transl Neurol 2023;10:32-47.
29. He C, Gong M, Li G, Shen Y, Han L, Han B, Lou M. Evaluation of White Matter Microstructural Alterations in Patients with Post-Stroke Cognitive Impairment at the Sub-Acute Stage. Neuropsychiatr Dis Treat 2022;18:563-73.
30. Zou Y, Murray DE, Durazzo TC, Schmidt TP, Murray TA, Meyerhoff DJ. White matter microstructural correlates of relapse in alcohol dependence. Psychiatry Res Neuroimaging 2018;281:92-100.
31. Nutt D, Hayes A, Fonville L, Zafar R, Palmer EOC, Paterson L, Lingford-Hughes A. Alcohol and the Brain. Nutrients 2021;13:3938.
32. Pfefferbaum A, Adalsteinsson E, Sullivan EV. Dysmorphology and microstructural degradation of the corpus callosum: Interaction of age and alcoholism. Neurobiol Aging 2006;27:994-1009.
33. Moeller FG, Hasan KM, Steinberg JL, Kramer LA, Dougherty DM, Santos RM, Valdes I, Swann AC, Barratt ES, Narayana PA. Reduced anterior corpus callosum white matter integrity is related to increased impulsivity and reduced discriminability in cocaine-dependent subjects: diffusion tensor imaging. Neuropsychopharmacology 2005;30:610-7.
34. Delisi LE, Bertisch HC, Szulc KU, Majcher M, Brown K, Bappal A, Ardekani BA. A preliminary DTI study showing no brain structural change associated with adolescent cannabis use. Harm Reduct J 2006;3:17.
35. Alhassoon OM, Sorg SF, Taylor MJ, Stephan RA, Schweinsburg BC, Stricker NH, Gongvatana A, Grant I. Callosal white matter microstructural recovery in abstinent alcoholics: a longitudinal diffusion tensor imaging study. Alcohol Clin Exp Res 2012;36:1922-31.
36. Yeo SS, Chang PH, Jang SH. The ascending reticular activating system from pontine reticular formation to

the thalamus in the human brain. Front Hum Neurosci 2013;7:416.
37. Wang Z, Wu W, Liu Y, Wang T, Chen X, Zhang J, Zhou G, Chen R. Altered Cerebellar White Matter Integrity in Patients with Mild Traumatic Brain Injury in the Acute Stage. PLoS One 2016;11:e0151489.
38. Ito K, Ohtsuka C, Yoshioka K, Maeda T, Yokosawa S, Mori F, Matsuda T, Terayama Y, Sasaki M. Differentiation Between Multiple System Atrophy and Other Spinocerebellar Degenerations Using Diffusion Kurtosis Imaging. Acad Radiol 2019;26:e333-9.
39. Pfefferbaum A, Sullivan EV. Microstructural but not macrostructural disruption of white matter in women with chronic alcoholism. Neuroimage 2002;15:708-18.
40. Newville J, Howard TA, Chavez GJ, Valenzuela CF, Cunningham LA. Persistent myelin abnormalities in a third trimester-equivalent mouse model of fetal alcohol spectrum disorder. Alcohol Clin Exp Res 2022;46:77-86.
41. Monnig MA, Yeo RA, Tonigan JS, McCrady BS, Thoma RJ, Sabbineni A, Hutchison KE. Associations of White Matter Microstructure with Clinical and Demographic Characteristics in Heavy Drinkers. PLoS One 2015;10:e0142042.
42. Sullivan EV, Pfefferbaum A. Diffusion tensor imaging in normal aging and neuropsychiatric disorders. Eur J Radiol 2003;45:244-55.
43. Charness ME. Brain lesions in alcoholics. Alcohol Clin Exp Res 1993;17:2-11.
44. Ma X, Coles CD, Lynch ME, Laconte SM, Zurkiya O, Wang D, Hu X. Evaluation of corpus callosum anisotropy in young adults with fetal alcohol syndrome according to diffusion tensor imaging. Alcohol Clin Exp Res 2005;29:1214-22.
45. Fryer SL, Schweinsburg BC, Bjorkquist OA, Frank LR, Mattson SN, Spadoni AD, Riley EP. Characterization of white matter microstructure in fetal alcohol spectrum disorders. Alcohol Clin Exp Res 2009;33:514-21.
46. Wozniak JR, Muetzel RL, Mueller BA, McGee CL, Freerks MA, Ward EE, Nelson ML, Chang PN, Lim KO. Microstructural corpus callosum anomalies in children with prenatal alcohol exposure: an extension of previous diffusion tensor imaging findings. Alcohol Clin Exp Res 2009;33:1825-35.
47. Skuja S, Groma V, Ravina K, Tarasovs M, Cauce V, Teteris O. Protective reactivity and alteration of the brain tissue in alcoholics evidenced by SOD1, MMP9 immunohistochemistry, and electron microscopy. Ultrastruct Pathol 2013;37:346-55.
48. Sippel HW. The acetaldehyde content in rat brain during ethanol metabolism. J Neurochem 1974;23:451-2.
49. Tang S, Xu S, Gullapalli RP, Medina AE. Effects of Early Alcohol Exposure on Functional Organization and Microstructure of a Visual-Tactile Integrative Circuit. Alcohol Clin Exp Res 2018;42:727-34.
50. Chen XR, Zeng JY, Shen ZW, Kong LM, Zheng WB. Diffusion Kurtosis Imaging Detects Microstructural Changes in the Brain after Acute Alcohol Intoxication in Rats. Biomed Res Int 2017;2017:4757025.
51. Morris LS, Dowell NG, Cercignani M, Harrison NA, Voon V. Binge drinking differentially affects cortical and subcortical microstructure. Addict Biol 2018;23:403-11.
52. Zhang H, Schneider T, Wheeler-Kingshott CA, Alexander DC. NODDI: practical in vivo neurite orientation dispersion and density imaging of the human brain. Neuroimage 2012;61:1000-16.
53. Zhang H, Hubbard PL, Parker GJ, Alexander DC. Axon diameter mapping in the presence of orientation dispersion with diffusion MRI. Neuroimage 2011;56:1301-15.
54. Pasternak O, Sochen N, Gur Y, Intrator N, Assaf Y. Free water elimination and mapping from diffusion MRI. Magn Reson Med 2009;62:717-30.
55. Özarslan E, Koay CG, Shepherd TM, Komlosh ME, İrfanoğlu MO, Pierpaoli C, Basser PJ. Mean apparent propagator (MAP) MRI: a novel diffusion imaging method for mapping tissue microstructure. Neuroimage 2013;78:16-32.
56. Papuć E, Rejdak K. The role of myelin damage in Alzheimer's disease pathology. Arch Med Sci 2020;16:345-51.
57. Avram AV, Sarlls JE, Barnett AS, Özarslan E, Thomas C, Irfanoglu MO, Hutchinson E, Pierpaoli C, Basser PJ. Clinical feasibility of using mean apparent propagator (MAP) MRI to characterize brain tissue microstructure. Neuroimage 2016;127:422-34.
58. Xie SH, Lang R, Li B, Zhao H, Wang P, He JL, Ma XY, Wu Q, Wang SY, Zhang HP, Gao Y, Wu JL. Evaluation of diffuse glioma grade and proliferation activity by different diffusion-weighted-imaging models including diffusion kurtosis imaging (DKI) and mean apparent propagator (MAP) MRI. Neuroradiology 2023;65:55-64.
59. Gao A, Zhang H, Yan X, Wang S, Chen Q, Gao E, Qi J, Bai J, Zhang Y, Cheng J. Whole-Tumor Histogram Analysis of Multiple Diffusion Metrics for Glioma Genotyping. Radiology 2022;302:652-61.
60. Crombe A, Planche V, Raffard G, Bourel J, Dubourdieu N, Panatier A, Fukutomi H, Dousset V, Oliet S, Hiba

B, Tourdias T. Deciphering the microstructure of hippocampal subfields with in vivo DTI and NODDI: Applications to experimental multiple sclerosis. Neuroimage 2018;172:357-68.
61. Andica C, Kamagata K, Hatano T, Saito Y, Ogaki K, Hattori N, Aoki S. MR Biomarkers of Degenerative Brain Disorders Derived From Diffusion Imaging. J Magn Reson Imaging 2020;52:1620-36.
62. Ma K, Zhang X, Zhang H, Yan X, Gao A, Song C, Wang S, Lian Y, Cheng J. Mean apparent propagator-MRI: A new diffusion model which improves temporal lobe epilepsy lateralization. Eur J Radiol 2020;126:108914.
63. Le H, Zeng W, Zhang H, Li J, Wu X, Xie M, Yan X, Zhou M, Zhang H, Wang M, Hong G, Shen J. Mean Apparent Propagator MRI Is Better Than Conventional Diffusion Tensor Imaging for the Evaluation of Parkinson's Disease: A Prospective Pilot Study. Front Aging Neurosci 2020;12:563595.

Cite this article as: Yi M, Wang T, Li X, Jiang Y, Wang Y, Zhang L, Chen W, Hu J, Wu H, Zhou Y, Luo G, Liu J, Zhou H. White matter microstructural alterations are associated with cognitive decline in benzodiazepine use disorders: a multi-shell diffusion magnetic resonance imaging study. Quant Imaging Med Surg 2025;15(3):2076-2093. doi: 10.21037/qims-24-1516

